Orbital engineering of two-dimensional materials with hydrogenation: A realization of giant gap and strongly correlated topological insulators

Anh Pham,[1,*] Carmen J. Gil,[1,2] Sean C. Smith,[3] and Sean Li[1]

[1]*School of Materials Science and Engineering, The University of New South Wales, Sydney NSW 2052, Australia*

[2]*School of Chemical Engineering, University of Florida, Gainesville, Florida 32611, USA*

[3]*Integrated Materials Design Centre, School of Chemical Engineering, The University of New South Wales, Sydney NSW 2052, Australia*

(Received 21 December 2014; revised manuscript received 20 May 2015; published 23 July 2015)

Orbital interaction plays an important role in topological insulators. Using first-principles calculations, we demonstrate that hydrogenation can change two-dimensional (2D) trivial insulator/semimetal-like Pb, Mo, and W to a Z_2 topological insulator with giant gaps by filtering unwanted orbitals such as the p_z orbital in Pb, and the $d_{3z^2-r^2}$ in Mo and W. For PbH, the large intrinsic spin-orbit coupling (SOC) confined in the in-plane orbitals $p_{x,y}$ results in a bulk gap of 1.07 eV. For the case of MoH and WH, hydrogenation results in a novel sd^4 hybridization with a Dirac cone formed by the out-of-plane orbital $d_{yz/xz}$ orbitals. Furthermore, due to the electron-electron interaction and the strong SOC in the 4*d* and 5*d* elements, the bulk band gap is significantly enhanced with a value of 1.28 eV for MoH and 0.30 eV for WH. The strong correlation effect also induces several topological phase transitions in WH like the Dirac semimetal and Mott insulating phase, while MoH remains a topological insulator even with large correlation effect. We propose that these new strongly correlated 2D materials can be realized experimentally by using substrate such as the boron nitride sheet, which can exhibit various novel properties such as the Dirac semimetal phase with large spin-orbit energy splitting as well as the quantum spin Hall property.

DOI: 10.1103/PhysRevB.92.035427 PACS number(s): 71.27.+a, 03.65.Vf, 31.15.A−, 81.65.Cf

I. INTRODUCTION

The novel two-dimensional (2D) topological insulating materials known as quantum spin Hall insulators (QSHIs) first predicted by Kane and Mele [1] have sparked off extensive research to develop this new class of materials. The 2D QSHIs are characterized by an insulating bulk state with metallic edge states [2–4]. Several 2D materials with quantum well structures [5–8] have been reported to be QSHIs, but their band gaps are not large enough for a wide range of practical applications. In the Kane-Mele model, the insulating bulk gap of a QSHI is determined primarily by the strength of the spin-orbit coupling (SOC). Based on this approach, new 2D materials, which are composed of heavy elements [9–11], have been studied as the candidates for large gap QSHIs. These materials all share a key feature: the bulk gap originates from either the next-nearest neighboring interaction in the p_z orbitals like in Si, Ge, and Sn, or the hoppings between p_x, p_y, and p_z orbitals like in Bi bilayer and III-Bi.

Recent studies have highlighted the importance of orbitals selection in determining the bulk energy gap [12–24]. For instance, stanene [12] has a small bulk gap of 0.1 eV when the p_z orbital dominates the effective low-energy band structure. However, through fluorination, the spin-orbit interaction can be confined on the in-plane p_x and p_y orbitals of stanene, thus enhancing its bulk gap to 0.3 eV. Other materials with large intrinsic spin-orbit coupling like Bi have also been demonstrated to contain above room temperature bulk gap using Si substrate as a tool of orbital filtering [14,15]. Furthermore, orbital filtering is also applicable in materials with asymmetric sublattices like III-Bi [22] and GaAs(111) [23] to generate QSHI with large Rashba effect. As a result, orbital filtering is demonstrated to be an effective technique to produce large gap QSHI in materials with *s* and *p* orbitals dominating the conduction and valence bands. This raises an interesting question: Can the orbital filtering effect be applied to materials with 4*d* and 5*d* orbitals?

In this paper, we address the aforementioned question by theoretically demonstrating the effect of hydrogenation as an effective tool to create QSHIs with giant gap and strongly correlated property. The paper is structured as follows: first we revisit the case of Pb in Sec. III A since it demonstrates the ability of hydrogenation to change the trivial insulating state of 2D Pb to a large gap QSHI. In Sec. III B 4*d* and 5*d* materials of group VI metals (Mo, W) were investigated due to the nature of their electronic structures. Specifically, in two dimensions the hexagonal crystal field can split the five *d* orbitals of Mo and W into three groups: two degenerate d_{xy} and $d_{x^2-y^2}$ orbitals, doubly degenerate d_{yz} and d_{xz} orbitals, and a singly degenerate $d_{3z^2-r^2}$ orbital. Due to this characteristic, the selection of a particular set of degenerate *d* orbitals is important to form a single band crossing at the Fermi level analogous to the sp^2 or sp^3 hybridization in group IV 2D QSHIs. Such a selection can be realized through hydrogenation to result in a novel sd^4 hybridization for materials like Mo and W. Most importantly, coupled with a strong spin-orbit coupling and the electron-electron interaction, this process produces new strongly correlated QSHIs with large gaps.

II. THEORETICAL METHOD

The calculations were performed using the projected augmented wave method [25]. A cut-off energy of 500 eV was used to expand the plane wave basis as implemented in the VASP package. A *k*-point mesh of $21 \times 21 \times 1$ was used within the Monkhorst-Pack method [26]. To optimize

*Corresponding author: anh.pham@unsw.edu.au

the geometrical structures, the lattice parameters and the internal ion coordinates were relaxed with the self-consistent criteria of 10^{-6} eV until the forces were less than 0.01 eV/Å. The calculations with and without the spin-orbit interaction were conducted using the Perdew-Burke-Ernzerhof exchange correlation functional [27]. The band gap of hydrogenated $4d$ and $5d$ were also investigated using the DFT + U method. Within the DFT + U functional, the Dudarev scheme was utilized [28] with an effective Hubbard potential U_{eff} defined as the difference between the Coulomb potential U and the on-site exchange interaction J, i.e., $U_{\text{eff}} = U - J$. The value of J is set to 0.5 eV in all calculations since within the Dudarev scheme only the U_{eff} value can affect the electron-electron interaction. We also tested the band gap of MoH and WH with different values of J such as 0.86 and 1 eV but they do not alter the final results. Different values of U_{eff} were investigated to study the topological properties and the bulk band gap. The single layer structures were constructed with a vacuum layer of 20 Å to avoid the interactions between the layers. For the nanoribbon configurations, we included a vacuum layer of 40 Å in the y and z directions to confine the structure in one dimension. To determine the Z_2 index of the inversion symmetric 2D materials, the parities of the 2N occupied bands were calculated by extracting the coefficients of the Kohn-Sham wave functions from the self-consistent WAVECAR. The parities were calculated at the four time-reversal invariant momenta: $\Gamma(0,0)$, $M_1(0, 0.5)$, $M_2(0.5, 0)$, and $M_3(0.5, 0.5)$. The topological invariant ν was determined based on the Fu-Kane's formula [29]: $(-1)^{\nu} = \prod \delta(M_i)\delta(\Gamma)$ where $\delta(M_i)$ and $\delta(K)$ are parities at M_1, M_2, M_3, and Γ, respectively. Due to the hexagonal symmetry, the parities at the three M points are identical, thus the topological invariant can be reduced to $(-1)^{\nu} = \delta^3(M)\delta(\Gamma)$.

III. RESULTS AND DISCUSSIONS

A. Effect of hydrogenation in Pb

We revisit the case of hydrogenated Pb to highlight the effect of orbital filtering via hydrogenation in p orbitals. The optimized 2D geometry and the band gap values of all the materials are summarized in Table I. For 2D hexagonal Pb, the structural optimization results in a low buckled structure. Figure 1(a) shows the band structure of an unhydrogenated Pb without and with the SOC effect. Without the SOC, an energy gap occurs at the K point between the $|p_z\rangle$ orbitals at the low energy level in contrast to other group IV QSHI such as Si, Ge [9], and Sn [12]. The absence of the Dirac point at K in 2D Pb can be attributed to the much weakened π bond which is composed of the hopping between the $|p_z\rangle$ orbitals. A single band crossing now occurs at the Γ point between the $|p_{x,y}\rangle$ states indicating the stronger σ bonding, and thus results in a higher buckling value in the geometrical structure as compared to materials such as silicene, germanene, and stanene. The $|p_z\rangle$ orbital is also observed at the Γ below the $|p_{x,y}\rangle$ orbitals at the Fermi level. When the SOC becomes effective, a large indirect bulk band gap of 0.494 eV occurs between the $|p_{x,y}\rangle$ orbitals at the Γ point and the $|p_z\rangle$ orbital at the K point. The SOC opens a band gap at the Γ point between the $|p_{x,y}\rangle$ orbitals, but it also lowers the energy level of the $|p_z\rangle$ orbital in the conduction band and thus results in an indirect band gap. Using the parity criteria, the topological invariant ν was calculated to be 0 [Fig. 1(a)], indicating a trivial insulating state of 2D Pb. As a result, strong SOC is not enough for the topological property. This trivial insulating property in low buckled Pb was observed by Huang *et al.* [30], who also demonstrated the persistence of the normal insulating state in 2D Pb with tensile strain or compression [30]. This intriguing property of Pb is significantly different from other group IV and V materials [31–33].

A topological phase transition occurs after Pb has undergone the hydrogenation process. After hydrogenation, the

TABLE I. Lattice parameters, buckling parameters d, bulk energy gap, and phase of the structures investigated in our study. The band gap and lattice were calculated within the density functional theory (DFT) method with SOC. The phase indicates whether the material is a normal insulator (NI)/normal semimetal (NSM), or a topological insulator (TI) based on the parity calculations.

System	Lattice (Å)	d (Å)	Energy gap (eV)	Phase
Mo	4.06	0	0.318	NI
MoH	4.09	0.097	0.19	TI
W	4.15	0	−0.117	NSM
WH	4.18	0.048	0.263	TI
Pb	4.93	0.924	0.494	NI
PbH	5.03	0.807	1.07	TI

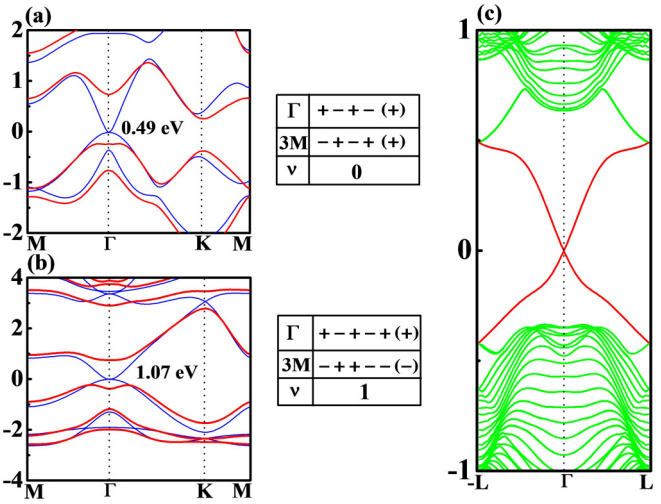

FIG. 1. (Color online) (a) Left: The band structure of 2D Pb without and with the SOC; the blue lines represent band structure without SOC and the red line represents band structure with SOC; the indirect bulk gap of 0.49 eV is also shown. Right: the corresponding parities at the TRIM point Γ and the three M points; the $+/-$ sign represents the even/odd parity. The parity in parentheses represents the product of the parities of all the occupied bands at Γ and M. (b) Left: the band structure of 2D PbH without and with the SOC; a direct bulk energy of 1.07 eV is also shown; the color scheme is similar to (a). Right: the corresponding parities of PbH at the TRIM point Γ and the three M points. (c) The band structure with the SOC of the armchair nanoribbon of PbH with a width of 9.6 nm; the red line shows the edge state.

chemical functionalization saturates the p_z orbital in PbH, which alters the parity at the M_i symmetry lines [Fig. 1(b)].The parities at M_1, M_2, and M_3 are now transformed from even (+) in Pb to odd (−) in PbH, which results in a nontrivial topological invariant $\nu = 1$. Further examination of the band structure shows that the bands near the Fermi level are dominated only by the $|p_{x,y}\rangle$ orbitals rather than a mixing of the $|p_z\rangle$ and the $|p_{x,y}\rangle$ orbitals as in 2D Pb, which explains the changes in the parities at the M points. In addition, the large SOC effect of Pb creates a giant direct energy gap of 1.07 eV occurring between the two even $|p_{x,y}\rangle$ states at the Γ point in PbH. 2D QSHI with $|p_{x,y}\rangle$ orbitals has also been observed in other Pb based 2D systems such as methyl modified bilayer Pb [21], and in hydrogenated and fluorinated Bi [16,18]. These results emphasize the importance of orbital selection for topological materials.

An important property of topological insulators is the helical edge state which is important for spintronic application due to the ability of QSHI to conduct dissipationless currents. To confirm the existence of the metallic state at the edges, the band structure of an armchair nanoribbon (ANR) PbH was calculated with the SOC effect. The nanoribbon has a width of 9.6 nm to avoid the interaction between the top and bottom edges. As demonstrated in Fig. 1(c), the edge states show a linear dispersion which further confirms the nontrivial topological properties of PbH. The Dirac point is located at the Fermi level, which opens up the possibility to tune the chemical potential which is above and below the Fermi level for practical electronic application.

B. Hydrogenation in 4*d* and 5*d* materials

For the materials containing 4*d* and 5*d* metals, we focus on group VI metals. Figure 2 shows the band structure of a graphene-like tungsten and molybdenum sheet. The

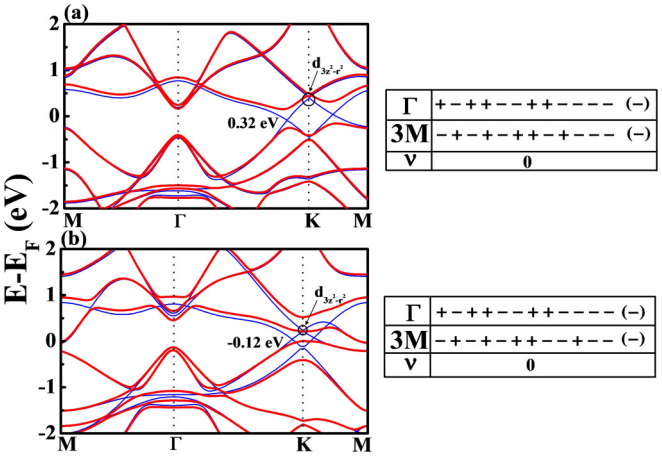

FIG. 2. (Color online) (a) Left: the band structure of 2D Mo with an indirect bulk gap of 0.32 eV with the SOC; the color line shows the effect of without and with SOC similar to Fig. 1(a). Right: the corresponding parities of all the occupied states of 2D Mo at the Γ and M points. (b) Left: the band structure of 2D W with an indirect bulk gap of −0.12 eV with the SOC; the color line shows the effect of without and with SOC similar to Fig. 1(a). Right: the corresponding parities of the occupied states of 2D W at the Γ and M points.

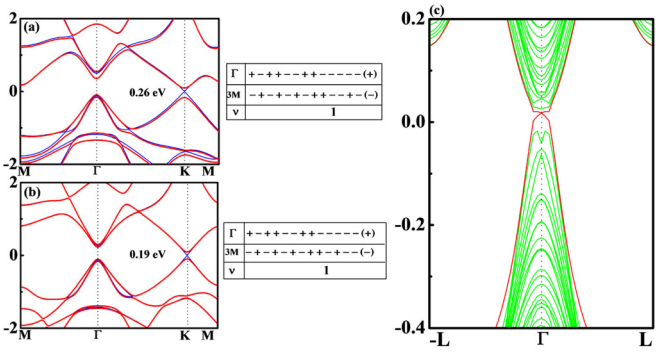

FIG. 3. (Color online) (a) Left: the band structure of 2D WH with an indirect bulk gap of 0.26 eV due to the SOC; the color lines show the effect of without and with SOC similar to Fig. 1(a). Right: the corresponding parities of WH at the TRIM point Γ and the three M points. (b) Left: the band structure of 2D MoH without and with the SOC; an indirect bulk energy of 0.19 eV is also shown. Right: the corresponding parities of MoH at the TRIM point Γ and M points. (c) The band structure with the SOC of the WH armchair nanoribbon with a width of 13.9 nm; the red line shows the edge state.

conduction and valence bands at the Γ point of 2D W are degenerate with a small energy gap, which mainly consists of the doubly degenerate d_{xy} and $d_{x^2-y^2}$. At the K point, the orbitals overlapping between the singly degenerate $d_{3z^2-r^2}$ and doubly degenerate d_{yz} and d_{xz} states form the four band crossings [Fig. 2(a)]. With the inclusion of SOC, the degeneracy at the Γ point is lifted while a gap occurs between the doubly degenerate d_{yz} and d_{xz}. However, 2D W still remains semimetallic due to the $d_{3z^2-r^2}$ being unaffected by the SOC. On the other hand, for the 2D hexagonal Mo [Fig. 2(b)], the $d_{3z^2-r^2}$ orbitals also contribute to the band crossing at the Fermi level at K, but the presence of the SOC leads to an energy gap opening between the $d_{yz/xz}$ and $d_{3z^2-r^2}$ states, resulting in an insulating state [Fig. 3(a)]. Since 2D hexagonal W and Mo are both nonmagnetic, we apply the parity criteria to calculate the topological invariant ν of 2D W and Mo [Figs. 2(a) and 2(b)]. The parities at Γ and the three M points are all odd, which results in a topologically trivial state ($\nu = 0$). Based on these results, it is possible to conclude that similar to 2D Pb, even though a band gap opening can occur due to the strong SOC, this does not guarantee the material is a topological insulator. Thus, to transform the topological properties of Mo and W, an orbital reconstruction needs to occur at the TRIM points (Γ or M).

To engineer the orbitals ordering in Mo and W, the surfaces of W and Mo are chemically modified with hydrogen in a ratio 1:1 similar to the modification applied on Pb, which filters out the $d_{3z^2-r^2}$ orbital. As demonstrated in Fig. 3(a), the band structure of WH reveals a single linear dispersion at the K point, which is composed of the doubly degenerate d_{yz} and d_{xz}, while the d_{xy} and $d_{x^2-y^2}$ states are still dominated at the Γ point. In this case, the effect of SOC causes a band gap opening with the topological invariant $\nu = 1$, making WH a Z_2 topological insulator. This topological phase transition occurs since the hydrogenation process saturates the $d_{3z^2-r^2}$ orbital, making it localized inside the valance band at the Γ point. Furthermore, this orbital reconstruction results in

a change in the parity at Γ from − to +, leading to a nontrivial topological insulating state in the presence of the SOC. Further examination of the band structure reveals the nontrivial behaviors at the Γ and K valleys, which determines the global band gap. At the Γ valley, the SOC lifts the degeneracy, which creates a large energy splitting in the bulk conduction and valence bands similar to that in the single layer transition-metal dichalcogenides [34–37]. This energy splitting is estimated to be 0.18 eV in the conduction band and 0.06 eV in the valence band. On the other hand, at the K point, SOC creates a band gap between the $|d_{yz,xz}\rangle$ states due to the intrinsically strong spin-orbit coupling in W. Similar behavior is also observed in MoH with the Z_2 index $\nu = 1$ indicating that MoH is also a quantum spin Hall insulator [Fig. 3(b)]. To further verify that WH is a QSHI, the band structure of 13.9 nm WH ANR was calculated with the SOC showing a single band crossing at Fermi level [Fig. 3(c)]. These results confirm that hydrogenation can effectively turn normal materials such as 2D Mo and W into topological insulators. In addition to Mo and W, other 4d and 5d elements neighboring group VI metals such as Zr, Nb, Hf, Re, Ta, and Ir in honeycomb lattices were also studied, but no topological insulating states were observed due to either the existence of strong magnetism or several band crossings existing at the Fermi level. In addition to the quantum spin Hall property, single sided hydrogenation on Mo and W was also studied because this can potentially generate the quantum anomalous Hall effect [20]. However, in the case of Mo and W, single sided hydrogenation still leaves the $d_{3z^2-r^2}$ at the Fermi level making these materials metallic.

Since the energy gap between the valence and conduction bands of the hydrogenated group VI metals is mainly composed of the doubly degenerate $|d_{yz,xz}\rangle$ states, this value is sensitive to the strongly correlated effect. To investigate the robustness of the topological property, the DFT + U method was utilized to investigate the effect of Hubbard potential U_{eff} on the band structure of WH and MoH [Figs. 4 and 5]. Different values of U_{eff} were used to simulate different strengths of the correlation effect. For WH, the global band gap increases monotonically as the value of U_{eff} increases from 0 to 2 eV

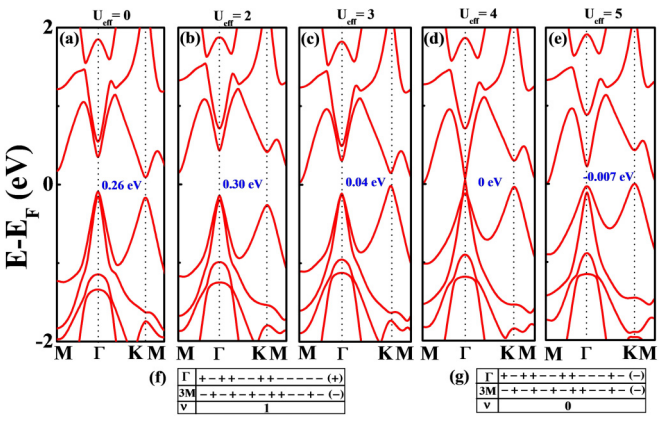

FIG. 4. (Color online) (a)–(e) The band structure of WH with the SOC and $U_{\text{eff}} = 0$, 2, 3, 4, and 5 eV, respectively; the global bulk band gap is indicated in blue. (f) The parities of Γ and M calculated with SOC + $U_{\text{eff}} = 0$, 2, and 3 eV. (g) The parities calculated with SOC + $U_{\text{eff}} = 5$ eV.

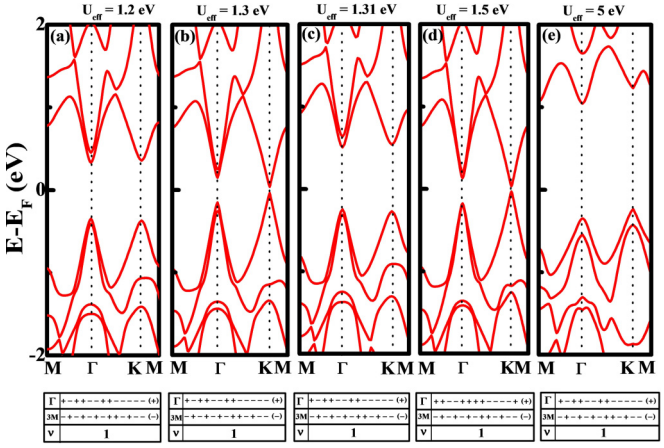

FIG. 5. (Color online) (a)–(e) Top: the band structure of MoH with SOC at $U_{\text{eff}} = 1.2$, 1.3, 1.31 , 1.5 and 5 eV. (a)–(e) Bottom: the corresponding parities of the occupied bands of MoH calculated at $U_{\text{eff}} = 1.2$, 1.3, 1.31, 1.5, and 5 eV.

(Fig. 4). The largest band gap value of 0.30 eV is achieved at $U_{\text{eff}} = 2$ eV. This implies that the topological property of WH is preserved since a topological phase transition will result in a band gap closing [38,39]. As demonstrated in the band structures, the inclusion of U_{eff} increases the band gap at the K point, while it also increases the energy splitting at the Γ point. Furthermore, it is important to notice that the correlation effect U_{eff} does not change the orbital characteristics of the TRIM points, i.e., the $d_{x^2-y^2}/d_{xy}$ orbitals still dominate the Γ point. However, as $U_{\text{eff}} > 2$ eV, the band gap starts to decrease which results in a Dirac semimetal at $U_{\text{eff}} = 4$ eV [Fig. 4(d)]. This result signals a topological transition from a topological nontrivial state to a normal insulating state. To test this theory, several values of $U_{\text{eff}} > 4$ eV was calculated. As demonstrated in Fig. 4(e), a large value of $U_{\text{eff}} = 5$ eV opens an energy gap at the Γ point, and the structure has a small negative global gap, with a topological invariant $\nu = 0$ indicating this is a normal insulating state. As a result, the strongly correlated effect can result in a nontrivial topological phase transition in WH depending on the strength of the electron-electron interaction which can destroy the topological property.

In the case of MoH, different values of U_{eff} can result in significant changes in the global band gap but there is no topological phase transition. It is important to emphasize that MoH remains nonmagnetic for all values of studied U_{eff} similar to the case of WH. As demonstrated in Fig. 5, the band gap widens as U_{eff} increases from 0 eV suggesting that MoH remains a topological insulator. The parity calculations at $U_{\text{eff}} = 1.2$ eV show $\nu = 1$, and confirms the topological insulating property. At $U_{\text{eff}} = 1.3$ eV, a Dirac dispersion occurs at the K point with a small gap due to the spin-orbit effect. Between $U_{\text{eff}} = 1.3$ and 1.5 eV, the band gap widens for values of $U_{\text{eff}} > 1.3$ eV and then decreases as U_{eff} reaches 1.5 eV, which forms a Dirac dispersion with a small gap similar to $U_{\text{eff}} = 1.3$ eV. Interestingly, no topological phase transition occurs between $U_{\text{eff}} = 1.3$ and 1.5 eV. As the value of U_{eff} is greater than 1.5 eV, the band gap of MoH increases monotonically. For a large value of $U_{\text{eff}} = 5$ eV, a giant bulk band gap (1.28 eV) is observed with a 0.2 eV energy splitting in

the valence band and 0.6 eV in the conduction band. In contrast to WH, the large value of $U_{\text{eff}} = 5$ eV does not alter the parity of MoH. Thus, MoH is a strongly correlated topological insulator with giant bulk gap and large spin-orbit splitting in the conduction and valence bands.

Finally, we discuss the possibility of experimentally realizing these novel two-dimensional materials. For materials like Pb, it has been theoretically demonstrated that substrates like SiH (111) [14–16] can be used as an effective tool to filter the p_z orbitals to create a large gap topological insulator based on the $p_{x,y}$ orbitals. In addition, high quality thin films of Pb have been experimentally grown on insulating substrates using the molecular beam epitaxial technique [40], thus opening up the possibility to integrate conventional growth technology to produce large gap QSHI with p orbitals. For the case of materials like Mo and W, we propose that the hexagonal boron nitride (BN) sheet can be used as a potential substrate to experimentally realize these novel strongly correlated 2D QSHIs. BN has a wide band gap and high dielectric constant, making it suitable to grow 2D materials with hexagonal lattice [41]. To demonstrate the effect of WH and MoH grown on BN, we study the band structure of WH on a single layer of BN. Figures 6(a) and 6(b) represent the two different geometrical arrangements of WH/MoH on BN ($\sqrt{3} \times \sqrt{3}$) supercell with a 3.6% lattice mismatch for WH. Since there is a weak interaction between W and BN via the van der Waals forces, the substrate cannot filter the $d_{3z^2-r^2}$ in W, as in the case of the p_z orbital when Pb is patterned on SiH [14–16]. Thus, hydrogen is added to the two W atoms on one side of the thin film to filter out the $d_{3z^2-r^2}$ at the Fermi level. Experimentally,

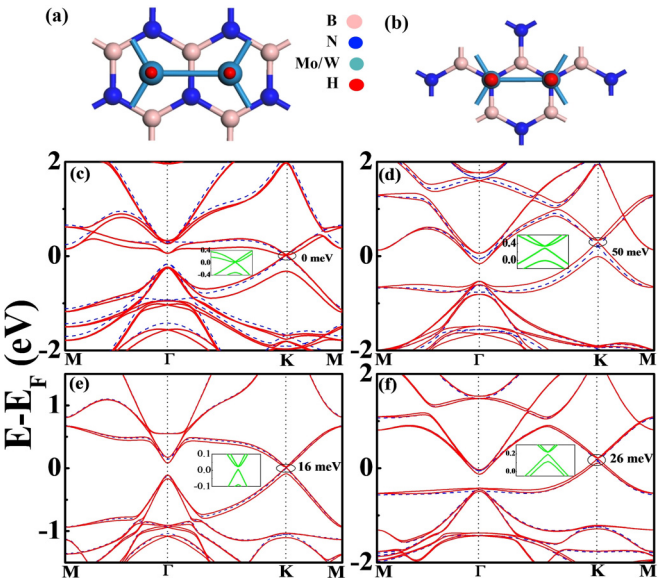

FIG. 6. (Color online) (a) and (b) The different geometrical arrangements of WH/MoH on the BN sheet. (c) and (d) The band structures of WH based on configuration (a) and (b), respectively. (d) and (e) The band structures of MoH based on configuration (a) and (b), respectively. The dashed blue line and thick red line show the effect of without and with SOC. The electronic bands with SOC at the K point of all the configurations are highlighted in the thick green lines.

the tungsten film can first be grown on a BN substrate, and then it is further treated with hydrogen in a 1:1 ratio using the established technique to fabricate graphane such as scanning tunneling microscopy assisted hydrogenation [42] or Ar-H_2 plasma [43].

The geometrical optimization was done using the density functional theory with van der Waals correction implemented in the DFT-D3 method [44]. The optimization results in a distance of 3.33 and 2.56 Å between WH and BN for configurations in Figs. 6(a) and 6(b), respectively. Based on the total energy, the configuration in Fig. 6(b) is shown to be more stable than that in Fig. 6(a). Interestingly, the different geometrical arrangement of WH on BN can also result in different electronic properties. When the WH atoms are arranged in the middle of the hexagonal BN ring [Fig. 6(a)], the band structure [Fig. 6(c)] shows a Dirac semimetal phase similar to graphene but with a large spin-orbit energy splitting at the K point. On the other hand, the more stable configuration in which the WH atoms are located above the B or N atoms in the BN substrate [Fig. 6(b)], produces a topological insulator [Fig. 6(d)] similar to the case of a freestanding WH. As demonstrated in Fig. 6(d), without the spin-orbit effect, a linear dispersion occurs at the K point which is dominated by the $d_{yz/xz}$ orbitals and a band gap opening occurs when the SOC is taken into account. On the other hand, for MoH grown on a BN sheet, the calculations show that the different geometrical arrangement of MoH on BN results in different values of the bulk gap [Figs. 6(e) and 6(f)] in the presence of the SOC, which suggests a type of inhomogeneous 2D QSHI. Based on these results, it is possible that by changing the fabricating condition, the electronic properties of 2D hydrogenated Mo/W grown on BN can be tuned to create a $4d/5d$ analogous of graphene, with a large spin-orbit splitting Dirac dispersion, or a topological insulating state.

It is also important to compare our results to the recent theoretical proposal of tungsten based sd^2 graphene, which exhibits the quantum anomalous Hall (QAH) effect with a 0.1 eV bulk gap [45]. Such a structure was realized by adsorbing W on Si(111) substrate decorated with Cl in a kagome lattice. The band structure of sd^2 W is composed of the s and the doubly degenerate in-plane $d_{xy}/d_{x^2-y^2}$ orbitals which intersect linearly to form the Dirac dispersion. While in hydrogenated W and Mo, the d_{yz}/d_{xz} orbitals contribute to the Dirac cone, with both the σ and π bondings occurring due to the contribution of the in-plane $d_{xy}/d_{x^2-y^2}$ orbitals as well as of the out-of-plane d_{yz}/d_{xz} orbitals, suggesting a sd^4 hybridization. This type of low-energy band structure resembles the sp^3 hybridization of group IV materials such as silicene, germanene, and stanene in which both the in-plane $p_{x,y}$ and out-of-plane p_z orbitals participate in the bondings, but the Dirac cone at the K point is only originated from the p_z orbitals. Thus, if the orbital ordering in Mo and W is engineered appropriately, exotic properties such as the QSH or QAH effects can be realized.

IV. CONCLUSIONS

In summary, we have demonstrated the effect of orbital filtering effect on p-based, and $4d$ and $5d$ materials through hydrogenation. Our results show that the hydrogenation

process can filter out the unwanted orbitals, which changes topologically trivial materials to Z_2 topological insulators with large gap. In the case of p-based materials such as Pb, the hydrogenation filters the p_z orbital which alters the parity at the M points from even to odd, thus resulting in a nontrivial topological invariant $\nu = 1$. Similarly, for $4d$ and $5d$ metallic elements such as Mo and W, hydrogen filters the $d_{3z^2-r^2}$ orbital which affects the parity at the Γ from $-$ to $+$, making MoH and WH 2D topological insulators with sd^4 hybridization. Furthermore, a combination of the large SOC and the strongly correlated effect result in a large bulk band gap of 1.28 eV for MoH and 0.30 eV for WH. Material such as WH also shows various topological phase transition from a topological insulating state to a Mott insulator based on the strength of the correlation effect, while for MoH the topological property is preserved even with large electron-electron interaction. The possibility of experimentally realizing WH and MoH using BN substrate was also considered. The calculations show that BN is a suitable substrate to generate exotic phenomenon such as the topological insulating state and the Dirac semimetal phase with large spin-orbit splitting at the Dirac cone. Based on these results, materials such as MoH and WH will facilitate further study into the interplay of the strongly correlated effect and the topological properties in 2D for future device applications.

ACKNOWLEDGMENTS

This research was supported by the Australian Research Council Discovery Projects, Future Fellowship and the LIEF grant. A.P. acknowledges the support of Professor Andrew Feenstra at Carnegie Mellon University for providing suitable codes to extract information from the WAVECAR binary file for parity calculation. C.J.G. acknowledges support for her contributions from the Buick Achievers Scholarship Program (General Motors Foundation), the American Chemical Society (ACS) Scholars Scholarship (American Chemical Society), and NSF IRES Award No. OISE-1129412. The computational resources were supported by Intersect Australia Ltd and the National Computing Infrastructure.

[1] C. L. Kane and E. J. Mele, Phys. Rev. Lett. **95**, 226801 (2005).
[2] M. Z. Hasan and C. L. Kane, Rev. Mod. Phys. **82**, 3045 (2010).
[3] X. L. Qi and S. C. Zhang, Rev. Mod. Phys. **83**, 1057 (2011).
[4] B. Yan and S. C. Zhang, Rep. Prog. Phys. **75**, 096501 (2012).
[5] B. A. Bernevig, T. L. Hughes, and S. C. Zhang, Science **314**, 1757 (2006).
[6] M. König, S. Wiedmann, C. Brüne, A. Roth, H. Buhmann, L. W. Molenkamp, X. L. Qi, and S. C. Zhang, Science **318**, 766 (2007).
[7] I. Knez, R. R. Du, and G. Sullivan, Phys. Rev. Lett. **107**, 136603 (2011).
[8] D. Zhang, L. Wenkai, M. Miao, S. C. Zhang, and K. Chang, Phys. Rev. Lett. **111**, 156402 (2013).
[9] C. C. Liu, W. Feng, and Y. G. Yao, Phys. Rev. Lett. **107**, 076802 (2011).
[10] Z. Liu, C.-X. Liu, Y.-S. Wu, W.-H. Duan, F. Liu, and J. Wu, Phys. Rev. Lett. **107**, 136805 (2011).
[11] F. C. Chuang, L. Z. Yao, Z. Q. Huang, Y. T. Liu, C. H. Hsu, T. Das, H. Lin, and A. Bansil, Nano. Lett. **14**, 2505 (2014).
[12] Y. Xu, B. Yan, H. J. Zhang, J. Wang, G. Xu, P. Tang, W. Duan, and S. C. Zhang, Phys. Rev. Lett. **111**, 136804 (2013).
[13] C. Si, J. Liu, Y. Xu, J. Wu, B.-L. Gu, and W. Duan, Phys. Rev. B **89**, 115429 (2014).
[14] M. Zhou, W. Ming, Z. Liu, Z. Wang, P. Lia, and F. Liu, Proc. Natl. Acad. Sci. USA **111**, 14378 (2014).
[15] M. Zhou, W. Ming, Z. Liu, Z. Wang, Y. Yao, and F. Liu, Sci. Rep. **4**, 7102 (2014).
[16] Z. Song, C.-C. Liu, J. Yang, J. Han, M. Ye, B. Fu, Y. Yang, Q. Niu, J. Lu, and Y. Yao, NPG Asia Mater. **6**, e147 (2014).
[17] K.-H. Jin and S.-H. Jhi, Sci. Rep. **5**, 8426 (2015).
[18] C.-C. Liu, S. Guan, Z. Song, S. A. Yang, J. Yang, and Y. Yao, Phys. Rev. B **90**, 085431 (2014).
[19] G. F. Zhang, Y. Li, and C. Wu, Phys. Rev. B **90**, 075114 (2014).
[20] C. Niu, G. Bihlmayer, H. Zhang, D. Wortmann, S. Blügel, and Y. Mokrousov, Phys. Rev. B **91**, 041303(R) (2015).
[21] Y. Ma, Y. Dai, L. Kou, T. Frauenheim, and T Heine, Nano Lett. **15**, 1083 (2015).
[22] Y. Ma, X. Li, L. Kou, B. Yan, C. Niu, Y. Dai, and T. Heine, Phys. Rev. B **91**, 235306 (2015).
[23] M. Zhao, X. Chen, L. Li, and X. Zhang, Sci. Rep. **5**, 8441 (2015).
[24] X. Zhang, H. Zhang, J. Wang, C. Felser, and S. C. Zhang, Science **335**, 1464 (2012).
[25] G. Kresse and D. Joubert, Phys. Rev. B **59**, 1758 (1999).
[26] H. J. Monkhorst and J. D. Pack, Phys. Rev. B **13**, 5188 (1976).
[27] J. P. Perdew, K. Burke, and M. Ernzerhof, Phys. Rev. Lett. **77**, 3865 (1996).
[28] S. L. Dudarev, G. A. Botton, S. Y. Savrasov, C. J. Humphreys, and A. P. Sutton, Phys. Rev. B **57**, 1505 (1998).
[29] L. Fu and C. L. Kane, Phys. Rev. B **76**, 045302 (2007).
[30] Z.-Q. Huang, C.-H. Hsu, F.-C. Chuang, Y.-T. Liu, H. Lin, W.-S. Su, V. Ozolins, and A. Bansil, New J. Phys. **16**, 105018 (2014).
[31] F. C. Chuang, C. H. Hsu, C. Y. Chen, Z. Q. Huang, V. Ozolins, H. Lin, and A. Bansil, Appl. Phys. Lett. **102**, 022424 (2013).
[32] L. Chen, Z. F. Wang, and F. Liu, Phys. Rev. B **87**, 235420 (2013).
[33] S. Küfner, M. Fitzner, and F. Bechstedt, Phys. Rev. B **90**, 125312 (2014).
[34] N. Alidoust, G. Bian, S.-Y. Xu, R. Sankar, M. Neupane, C. Liu, I. Belopolski, D. X. Qu, J. D. Denlinger, F.-C. Chou, and M. Z. Hasan, Nat. Commun. **5**, 5673 (2014)
[35] K. Kośmider, J. W. González, and J. Fernández-Rossier, Phys. Rev. B **88**, 245436 (2013).
[36] A. Kormanyos, V. Zolyomi, N. D. Drummond, P. Rakyta, G. Burkard, and V. I. Falko, Phys. Rev. B **88**, 045416 (2013).
[37] T. Cheiwchanchamnangij and W. R. L. Lambrecht, Phys. Rev. B **85**, 205302 (2012).
[38] X. Wan, A. M. Turner, A. Vishwanath, and Sergey Y. Savrasov, Phys. Rev. B **83**, 205101 (2011).

[39] X. Wan, A. Vishwanath, and S. Y. Savrasov, Phys. Rev. Lett **108**, 146601 (2012).

[40] Y. Guo, Y.-F. Zhang, X.-Y. Bao, T.-Z. Han, Z. Tang, L.-X. Zhang, W.-G. Zhu, E. Wang, Q. Niu, Z. Qiu *et al.*, Science **306**, 1915 (2004).

[41] L. Britnell, R. Gorbachev, R. Jalil, B. Belle, F. Schedin, A. Mishchenko, T. Georgiou, M. Katsnelson, L. Eaves, S. Morozov *et al.*, Science **335**, 947 (2012).

[42] N. P. Guisinger, G. M. Rutter, J. N. Crain, P. N. First, and J. A. Stroscio. Nano Lett. **9**, 1462 (2009).

[43] M. Wojtaszek, N. Tombros, A. Caretta, P. H. M. van Loosdrecht, and B. J. van Wees, J. Appl. Phys. **110**, 063715 (2011).

[44] S. Grimme, J. Antony, S. Ehrlich, and S. Krieg, J. Chem. Phys. **132**, 154104 (2010).

[45] M. Zhou, Z. Liu, W. Ming, Z. Wang, and F. Liu, Phys. Rev. Lett. **113**, 236802 (2014).